# An experimental study of the circular internal hydraulic jump

Iva Kavčič[1]

*University of Zagreb, Croatia*

Advisor: Steve Thorpe

*Bangor University, Wales, UK*

**Abstract.** The results of an experimental investigation of the circular internal hydraulic jump in two-layer fluid are presented, with focus on the dependence on the flow rates and density differences between fresh and salty water used. For the lower flow rates the stable circular patterns, consisted of three or four well-formed stationary waves, were observed, while for the higher flow rates their axial symmetry was lost by deformation of entire wave pattern in cusp-like features. This stable, laminar regime lasted 4-5 minutes, after which instabilities started to develop, finally breaking the wave patterns in turbulent motion. The radii of stationary waves were measured, and the depths of the fluid inside and outside the jump were calculated in order to find the critical values of jump radius, fluid depth and Froude number just before the onset of instabilities. While the values of jump radius, fluid depth and Froude number inside the jump (reaching values of up to 12-14) strongly depend on variations in flow rate and density difference, this dependence does not seem to be so strong for the Froude number outside the jump. Their values are below 1, due to dispersion relation for the internal waves in two-layer fluid used to calculate the fluid depth outside the jump. Comparison of results with the analytic Watson's (1964) model for the jump in the single-layer flow indicates the existence of similar functional dependence for the two-layer fluid. Finally, the experiments where the sharp density difference was smoothed by diffusion indicate that the stationary, laminar waves cannot occur in a continuously stratified fluid.

**Keywords:** Hydraulic jump; Stationary waves; Stratified fluid

## 1. Introduction

The circular hydraulic jump may arise when a fluid jet falling vertically at moderate Reynolds number strikes a horizontal plate (a usual fluid dynamics phenomenon, for instance often observed in a kitchen sink). Fluid is spread radially in a thin layer, until reaching a radius at which the layer depth increases

[1] E-mail: ivakavc@gfz.hr

abruptly. Theoretical predictions for the jump radius based on inviscid theory were first presented by Rayleigh (1914) in a paper on hydraulic jumps and bores. The dominant influence of fluid viscosity on the jump radius was elucidated by Watson (1964), who developed an appropriate description of the boundary layer on the impact plate. Watson (1964), however, has not accounted for another important influence on the jump radius in single-layer flow: the surface tension. Bush and Aristoff (2003) reviewed Watson's study of the circular hydraulic jump, and later illustrated the influence of surface tension on the jump radius in their experimental study (Bush et al., 2006). Subsequent studies of the circular jump have focused principally on describing the boundary layer separation and closed circulation cells ("rotors"), which may cause the changes of surface slopes and stable shapes other than circular, especially when fluids other than water are used (Watson, 1964; Craik et al., 1981; Bowles and Smith 1992; Bohr et al., 1993; Higuera, 1994; Bush and Aristoff, 2003; Bush et al., 2006).

The surface tension, however important it may be in the single-layer jumps, is negligible at the interface between the layers in the internal circular hydraulic jumps. These are produced when a denser fluid falls vertically onto a horizontal surface submerged beneath a deep layer of less dense, miscible fluid, radially spreading from the point of impact, at the typical distance of a few centimetres from it. Recent theoretical and numerical studies of internal hydraulic jumps in stably stratified two-layer miscible flows have been focused on the entrainment and mass transfer between the layers (Holland et al., 2002), and development of the proper parameterizations for description of energy dissipation in turbulent flows (Hassid et al., 2007). As seen from above, continuously stratified fluids are often represented as being in two layers. The subject of whether the stationary internal hydraulic jumps can occur in a stratified flow beneath of an unstratified stationary layer may be of some importance in relation to the jumps of much greater size that are postulated to occur in flows through channels on the flanks of mid-ocean ridges and through passages connecting the deep ocean basins (Thurnherr et al., 2005; Thorpe, 2007), although there are as yet no observations with sufficient resolution to establish the presence or otherwise of such transitions. Another example of what is described as the stationary internal hydraulic jump in the lee of The Sierra Nevada can be found in the book of Lighthill (1978; his Fig. 117).

This experimental study of the circular internal hydraulic jump attempts to gain insight in this interesting problem and to answer to some of the above questions, extending experimental work with two-layer fluid conducted by S. A. Thorpe. The report is organized as follows: first, a description of the experimental apparatus, with the details of representative experiments and observed jump patterns is given in Section 2. The calculated quantitative parameters are described in Section 3, followed by the conclusions and recommendations for future experiments in Section 4.

## 2. Experiments and observations

### 2.1. Experimental set-up

The simplified sketch of apparatus is given in Fig. 1. Salty water of density $\rho_2$ was pumped (Fig. 1, 5) from the bucket (Fig. 1, 6) through the nozzle of radius $a_{noz}$ = 0.113 cm (Fig. 1, 3) into the square glass tank (Fig. 1, 1; tank dimensions were 58.4×58.4 cm). Prior to the start of experiment it was necessary to establish the uniform flow of salty water by removing the bubbles of air. For that purpose an additional plastic tube with the T-junction (Fig. 1, 4) was used, directing the salty water in another bucket until the bubbles went out of the plastic tube. After that the flow was redirected to the nozzle for a few moments to push out the air from it. The nozzle was elevated to the height of about 0.3 cm from the tank bottom (to minimize any mixing between the descending with the surrounding fluid). Then, the tank was filled with fresh water of density $\rho_1$ to a depth of 3 cm, and left undisturbed for 15-20 minutes so the water could come to rest.

The pump was calibrated for the range of flow rates ($Q$) from 0.95-8.8 $cm^3s^{-1}$ (pump settings 0-999). However, it was observed that their values were somewhat smaller with the full experimental setup. Apparently, the small nozzle radius, rather than the higher density of salty water used in experiments mostly affected the flow rate. The density of fresh water was almost constant through all experiments ($\rho_1 \approx 0.99825$ $gcm^{-3}$). A plastic plate (Fig. 1, 2), covered with paper, was used both as support for the nozzle (in order to ensure that the impinging fluid was perpendicular to the tank bottom) and as the shadowgraph screen for observing and recording the observed patterns. They were made visible by the parallel light beam projected (Fig. 1, 9) onto (and reflected from) the mirror (Fig. 1, 7) below the tank, angled at $\alpha$ = 45° from the horizontal, and recorded with the Nikon digital photo camera (Fig. 1, 8) placed on the ladder above the tank. The photo of experimental setup is given in Figure 2 (camera not shown).

The range of flow rates used (also measured), and the corresponding speeds ($v_{noz}$) and Reynolds number ($Re_{noz}$) of flow in the nozzle are shown in Table 1. Here the Reynolds number is calculated as

$$Re_{noz} = \frac{v_{noz} a_{noz}}{\upsilon}, \tag{1}$$

where

$$v_{noz} = \frac{Q}{a_{noz}^2 \pi}, \tag{2}$$

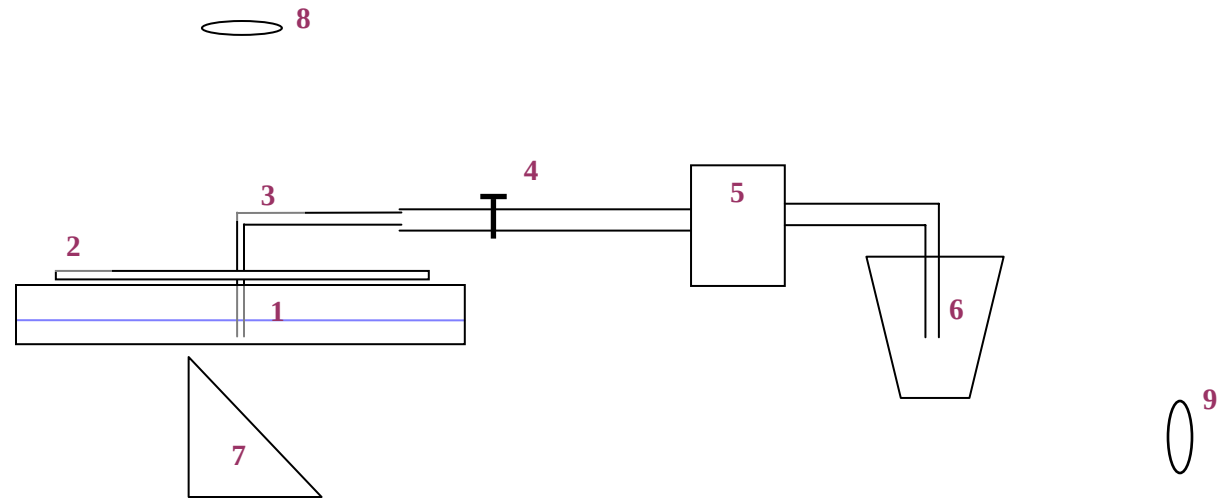


*Figure 1.* The simplified sketch of experimental apparatus: 1. Square tank: $a_t$ = 58.4 cm, $h_t$ = 5 cm, filled with fresh water ($\rho_1$); 2. Screen; 3. Nozzle ($a_{noz}$ = 0.113 cm), at $d_a$ = 0.3 cm; 4. Plastic tube with T-junction; 5. Pump; 6. Bucket with salty water ($\rho_2$, $\rho_2 > \rho_1$); 7. Mirror, $\alpha$ = 45°; 8. Camera; 9. Projector

| Setting | Q ($cm^3s^{-1}$) | $v_{noz}$ ($cms^{-1}$) | $Re_{noz}$ |
|---|---|---|---|
| 50 | 0.398 | 9.917 | 111.64 |
| 100 | 0.828 | 20.625 | 232.20 |
| 150 | 1.258 | 31.332 | 352.73 |
| 200 | 1.675 | 41.720 | 469.68 |
| 250 | 2.101 | 52.343 | 589.27 |
| 300 | 2.520 | 62.790 | 706.89 |

*Table 1.* Flow rates, flow speeds in the nozzle and Reynolds number of the flow in nozzle.

**a)**

**b)**

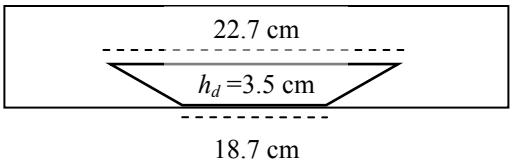


*Figure 2.* (a) The photo of experimental setup; (b) Pie dish used to simulate the circular geometry, with $h_d$ denoting its height.

and $\nu = 1.004\times10^{-6}$ $m^2s^{-1}$ is the value of kinematic viscosity of fresh water at 20 °C. Since the range of temperature of both fresh and salty water used in these experiments was approximately 18–23 °C, and the salty water was on average about 5-10 % denser than fresh, the above value of kinematic viscosity can be used with reasonable accuracy.

Two sets of experiments were made: the first with the higher density of salty water ($\rho_2 \approx 1.10544$ $gcm^{-3}$) for all flow rates in Table 1, and second using $\rho_2 \approx 1.05044$ $gcm^{-3}$, for pump settings 100 and 200. Each of them (apart from the one with the highest flow rate, 300), was performed at least twice: once in the square tank, and the other time with the Pyrex glass pie dish (put into the tank, dimensions and geometry shown in Fig. 2a) needed to simulate the radially symmetric boundaries. When conducting experiments with the pie dish, the initial height of fresh water was set at about 4 cm (≈ 5 mm deeper than the height of the pie dish) so that the fresh water covered its edge. When emptying the tank at the end of the experiment, it was observed that in the case of lower flow rates (settings 50-200) almost all of the salt water remained in the pie dish. Fresh water was effectively pushed out by salty water without the return circulation over the dish edge. At the higher flow rates (settings 250–300) filling of the dish with salty water was quick, initializing relatively fast overflow over the dish edge and corresponding inflow of the fresh water.

### 2.2. Development of the circular jump

As can be seen from Table 1, the experiments were conducted in the range of moderate Reynolds numbers (order $10^2$ - $10^3$). After the preparations, described in Section 2.1, the flow of salty water was switched on. It produced a radially spreading density current that eventually reached the side walls and in which, at a few centimetres from the impinging jet, stationary circular waves were formed. Due to the difference in refractive indices of fresh and salty water it was possible to distinguish between the crests (bright bands) and troughs (dark bands) of stationary waves that formed the transition region between the interior and exterior flow. The time evolution of typical observed wave patterns is shown in Figs. 3 (an example for the square tank) and 4 (an example for the pie dish). In the square tank stationary waves were formed within first 10 s after the start , with radii from 0.8 to 3.5 cm (Fig. 3a, shown after ≈ 3 min after the start of experiment). When the pie dish was used, the wave patterns were formed ≈ 30 s after the start of experiment (Fig. 4a), with the similar range of wave radii.

In the first set of experiments ($\rho_2 \approx 1.10544$ $gcm^{-3}$), for both square tank and pie dish, the observed waves were circular for the pump settings 50-200 (see Table 1 for the corresponding $Q$ and $Re_{noz}$) and formed of three (settings 50-150) or four bright rings (setting 200). The same was observed in the second set when the lower density ($\rho_2 \approx 1.05044$ $gcm^{-3}$) was used for flow rate $Q_{100}$ (Fig. 3a). When

the flow rate was increased to $Q_{250}$ = 2.101 $cm^3s^{-1}$ in the first, or to $Q_{200}$ = 1.675 $cm^3s^{-1}$ in the second set of experiments, the axial symmetry was lost in the cusp-like deformations (Fig. 4a). The higher flow rates ($Q_{300}$ and $Q_{250}$, for the first and second set of experiments, respectively) lead to wave breaking almost instantly after the flow of salty water started. Since they could not produce stable laminar wave patterns in the experiments presented, they are not discussed in this report. Also, the symmetry of waves was, even at the lower flow rates, extremely sensitive to any variations from horizontal; consequently, great care was taken in levelling the system. The white spot in Figs. 3 and 4 is a hole drilled in the plastic plate, through which potassium permanganate was added in most of the experiments in order to detect a possible appearance of boundary layer separation and rotors. Although we did not observe any clear indication of rotors, potassium permanganate was very useful in determining the general circulation patterns in the tank or the pie dish.

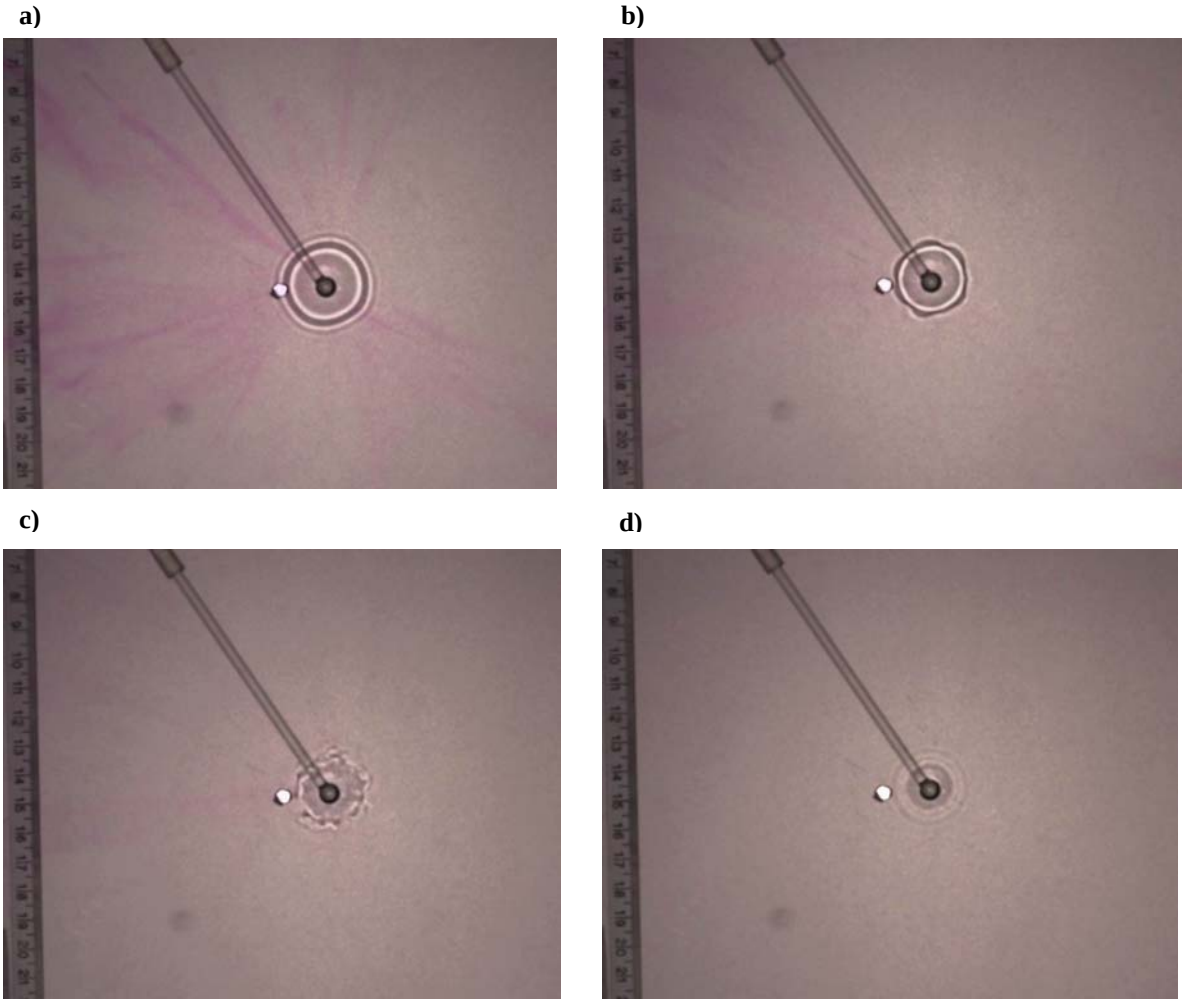


*Figure 3.* Observed jump patterns in the square tank at (a) 3 min 10 s, (b) 6 min, (c) 9 min 50 s and (d) 21 min 58 s after the start of experiment. Here $Q_{100}$ = 0.828 $cm^3s^{-1}$, $Re_{noz}$ = 232.20 and $\rho_2$ = 1.05058 $gcm^{-3}$.

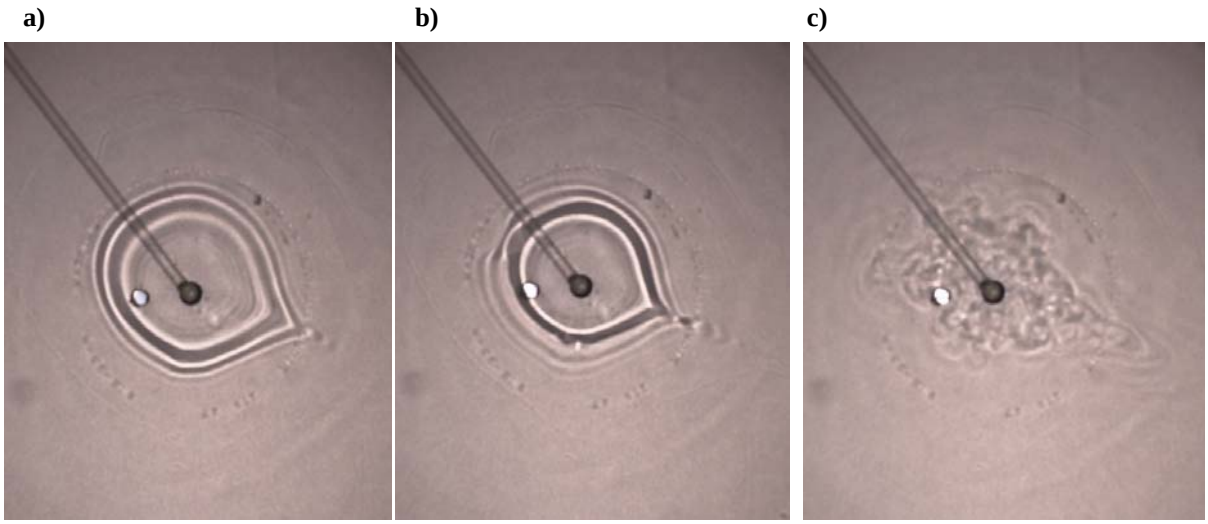


*Figure 4.* Observed jump patterns in the pie dish (a) 36 s, (b) 40 s and (c) 1 min after the start of experiment. Here $Q_{250}$ = 2.101 cm$^3$s$^{-1}$, $Re_{noz}$ = 589.27 and $\rho_2$ = 1.10511 gcm$^{-3}$. The size of photos is ≈ 10 cm×14 cm

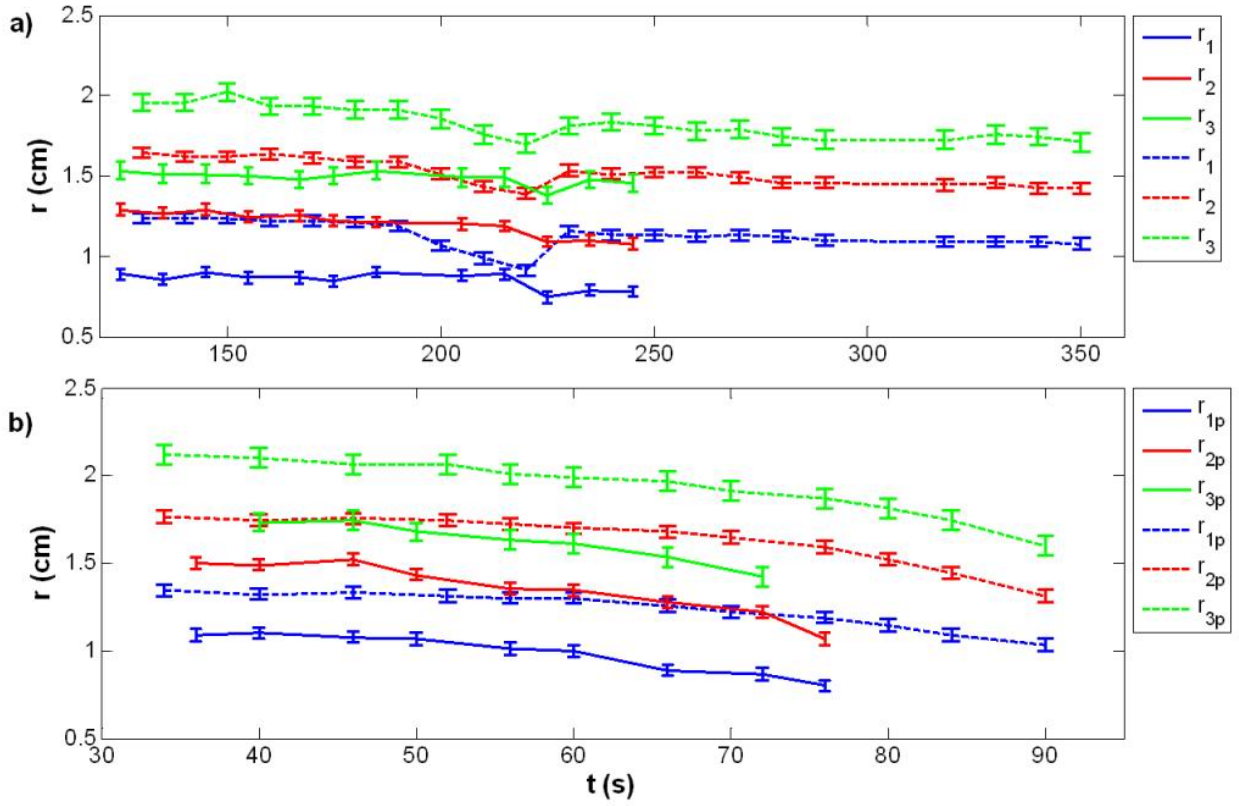


*Figure 5.* Time evolution of the standing wave radii (with error bars) for the pump setting 100: (a) without, and (b) with the pie dish for $\rho_2$ = 1.10527 gcm$^{-3}$ (solid) and $\rho_2$ = 1.05058 gcm$^{-3}$ (dashed). Here $Q_{100}$ = 0.828 cms$^{-1}$ and $Re_{noz}$ = 232.20; $r_1$ and $r_3$ are the radii of the innermost and outermost waves, respectively.

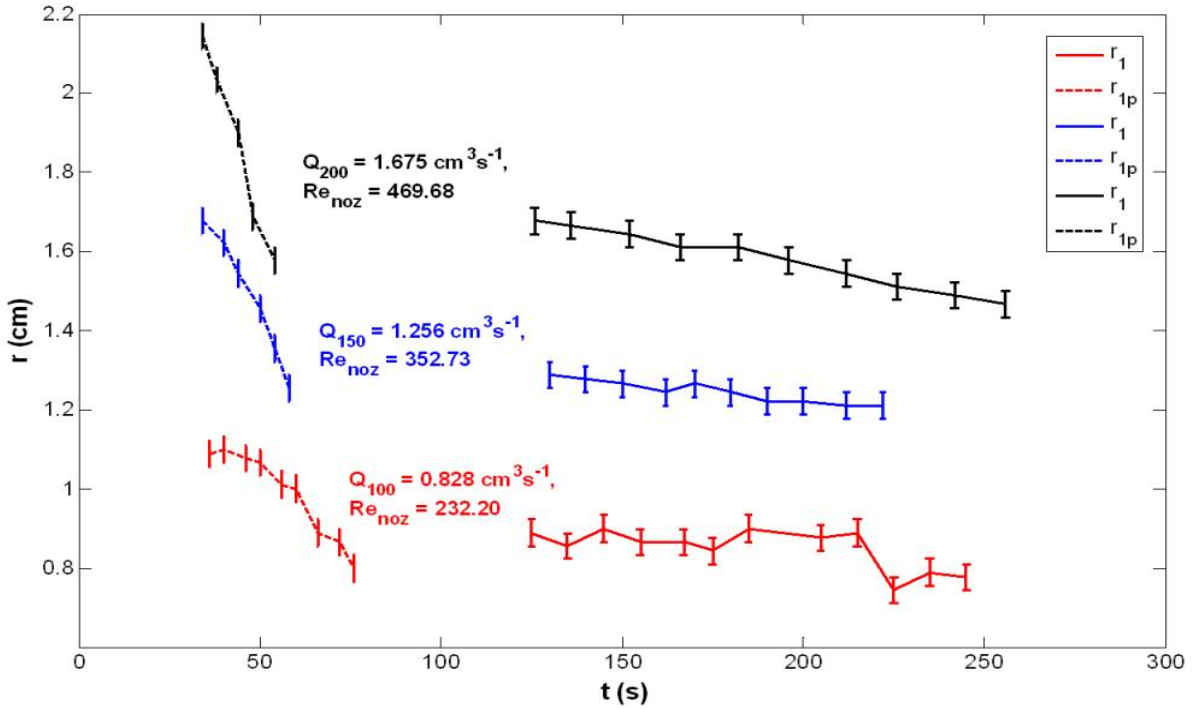


*Figure 6.* Time evolution of the innermost wave radius (with error bars), $r_1$, for the pump settings 100 (red, $\rho_2$ = 1.10527 gcm$^{-3}$), 150 (blue, $\rho_2$ = 1.10552 gcm$^{-3}$) and 200 (black, $\rho_2$ = 1.10507 gcm$^{-3}$), for the experiments without (solid) and with the pie dish (dashed).

The photos were processed by digitally extracting the cross-sections of wave patterns and detecting the positions of light maxima (in pixels), which then gave the estimates of the wave crests radii. To convert the radii from pixels to centimetres the translucent plastic ruler attached on top of the plastic plate (Fig. 1, 2, and Fig. 3) was used as the scale (at the resolution of photos used in experiments, 1 cm ≈ 45 pixels). Figure 5 shows the time evolution of wave crests radii ($r_1$, $r_2$, and $r_3$, respectively) for the flow rate $Q_{100}$, for both the higher (solid) and lower (dashed) density of salty water. In this, and all following plots as well, the results are shown after the time needed for the salty water to completely cover the bottom of the tank (≈ 2 min, Fig. 5a) or the pie dish (≈ 30 s, Fig. 5b), so the waves could be considered as quasi-stationary. The error bars (vertical ticks in plots) were calculated from the estimated uncertainties in determining the crests radii (± 2 pixels ≈ ± 0.04 cm for the inner waves, due to the stronger and thus better resolved light maxima, and ± 3 pixels ≈ ± 0.07 cm for the outer waves). It can be seen (Fig. 5) that the distance between the rings decreases as their radii increase, independently of the density difference, flow rate or geometry used. Also, the decreased density difference between fresh and salty water is responsible for increasing the wave radii for the same flow rate (Fig. 5, dashed lines). In Figure 6 a similar comparison is given for the various flow rates at the same density difference (only the innermost

radius, $r_1$, is shown), showing that increasing the flow rate (from $Q_{100}$ to $Q_{200}$) results in increase of wave crests radii (red, blue and black lines, respectively). Both Figures 5 and 6 show the main difference between the experiments without and with the pie dish, i.e. when the pie dish was used, the greater wave radii were observed, but their decreasing with time was faster (due to the faster filling with salty water). This rapidity of changes brings into question the assumption of waves being stationary in the pie dish, although the same assumption is valid in the square tank.

### 2.3. Transition from steady wavelike to turbulent flow

The stable wave patterns, described in Section 2.2, lasted for approximately 4 min for the salt solution of higher, and 5 min for the solution of lower density (Fig. 3a). After that time the outer band was deformed by the irregular undular instabilities moving around it, while the inner waves were still visible (Fig. 3b). After ≈ 1 min for the solution of higher, i.e. ≈ 1.5 – 2 min for the solution of lower density (Fig. 3c) the inner waves also collapsed and the motion became turbulent. This motion appeared to be organized in the forms looking alike the flower petals that were moving in groups around, and bursting in and out of the deformed outer band (Fig. 3c). As the turbulent mixing decreased the density differences, the flow eventually calmed (Fig. 3d). Experiments with the tank only therefore lasted from 30-50 min (depending on the flow rate) and the photos were taken initially every 10 s, and after that every 15-30 s as the flow became steadier. When the pie dish was used, the onset of instabilities was after ≈ 1 min after the start of experiment (Fig. 4b). Also, the transition between the laminar and turbulent regime happened almost instantly (within a few seconds), leading to the well developed turbulent forms (Fig. 4c). Because of the faster dynamics photos were initially taken every 5 s, and later every 10-15 s, and experiments lasted approximately 5 min.

The last values of wave crests radii in Figs. 5 and 6 are those estimated just before the onset of undular instabilities deformed the outermost wave (Figs. 3b and 4b). They, and all the parameters that will later be derived from them, will be referred as the "critical values". Besides increasing the wave radii for the same flow rate, it can be seen that the decreased density difference between fresh and salty water also postpones the onset of instabilities. For the flow rate $Q_{100}$ ($Re_{noz}$ = 232.20), in the square tank the radii of last undisturbed waves were estimated 240 s after the start of experiment for $\rho_2 \approx 1.10544$ gcm$^{-3}$ (Fig. 5a, solid), and 350 s for $\rho_2 \approx 1.05044$ gcm$^{-3}$ (Fig. 5a, dashed). As commented in Section 2.2, the duration of stable regime is shorter when the pie dish is used in experiments (Fig. 5b; ≈ 76 s for $\rho_2 \approx$ 1.10544 gcm$^{-3}$, solid, and 90 s for $\rho_2 \approx 1.05044$ gcm$^{-3}$, dashed). Interestingly, the onset of instabilities does not seem to depend on the increase of flow rates, and therefore the Reynolds numbers of the flow (Fig. 6).

### 2.4. Experiments with continuous stratification

The experiments in two-layer fluid, described above, were later modified in order to investigate whether the internal hydraulic jump can occur in a continuously stratified fluid. Two such experiments were made (only in the pie dish, at $Q_{150}$ = 1.258 $cm^3s^{-1}$ and $Re_{noz}$ = 352.73), one for each mean density of salty water used ($\rho_2 \approx$ 1.10544 $gcm^{-3}$ and $\rho_2 \approx$ 1.05044 $gcm^{-3}$). To cover the distance between the nozzle and the pie dish bottom (about 3 mm of depth), the pie dish was initially filled with the salty water for approximately 85 s. This layer of salty water was then let to diffuse for at least two hours so the continuous density gradient between it (below) and fresh water (above) could be established. Since the above layer of fresh water was ≈ 3 cm thick, it could be considered as being of uniform density. After that, the experiment was conducted as usual, and the observations were compared to the former ones with the same flow rate and sharp density interface. In both of these experiments, independently of density difference or flow rate used, no stable laminar wave patterns as in previous experiments were observed. Instead, the diverging flow instantly became turbulent with no appearance of a stationary, laminar, circular jump surrounding the point of impact of the jet on the horizontal plane. Figure 7 shows the comparison of experiments with sharp density discontinuity (two-layer fluid, Fig. 7a), and with the continuous stratification in the lower layer (Fig. 7b), both at ≈ 45 s after the start of experiment. According to these observations, the stationary, laminar hydraulic jump cannot be sustained in a continuously stratified layer in motion beneath a stationary layer of uniform density.

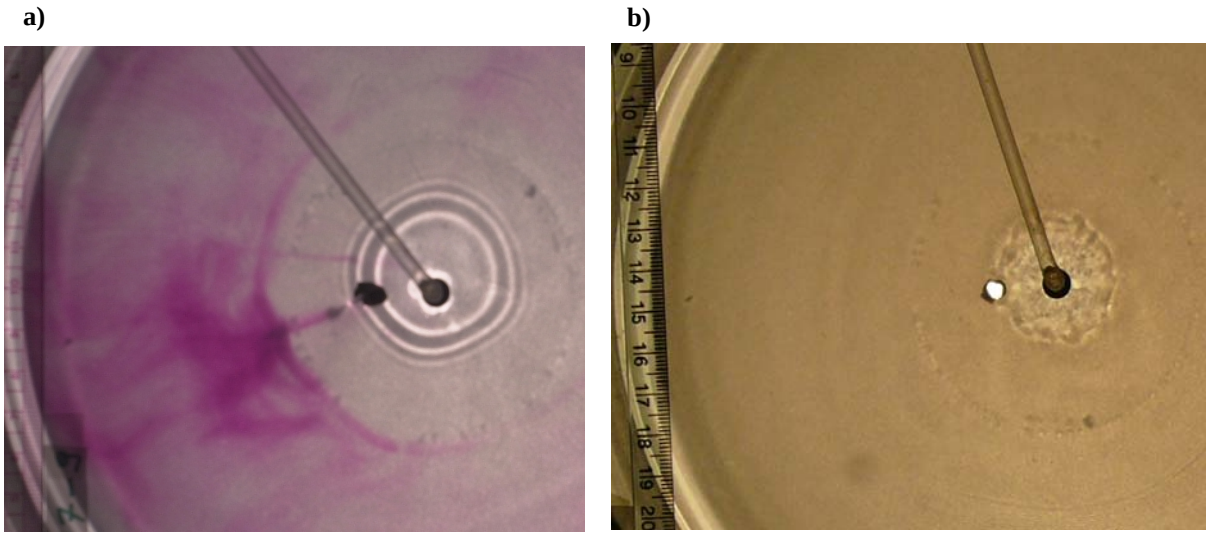


*Figure 7.* Observed jump patterns in the pie dish (a) in two layer fluid, and (b) with continuous stratification in the upper layer, both at ≈ 45 s after the start of experiment. Here $Q_{150}$ = 1.258 $cm^3s^{-1}$, $Re_{noz}$ = 352.73 and $\rho_2 \approx$ 1.10544 $gcm^{-3}$.

## 3. Parameter study

In this section we try to describe the observations in terms of some common parameters, which may also lead us to the conditions necessary for the development of instabilities in wave patterns. Furthermore, in Sec. 2 we saw that the difference in geometry of the problem (i.e. using the pie dish in experiments) affects the dynamics of observed waves. That brings us to the question: which are the common characteristics of these two types of experiments? As in Sec. 2, we will carry out this analysis first for the fixed density difference and different flow rates, and then we will compare results for the chosen flow rate, but with different densities of salty water. The main parameters we will use to describe the flow are:

1. Froude number inside (upstream), $Fr_1$, and outside (downstream) the jump, $Fr_2$. Here they are defined as

$$Fr_{1,2} = \frac{U_{1,2}^2}{g'H_{1,2}}. \tag{3}$$

$U_1$ and $U_2$ are the flow speeds inside and outside the jump, respectively, $H_1$ and $H_2$ are the corresponding depths of salty water, and $g'$ is the reduced density. $U_{1,2}$ and $g'$ can be calculated as:

$$U_{1,2} = \frac{Q}{2\pi R_{1,2} H_{1,2}}, \tag{4}$$

$$g' = g\delta_\rho, \;\; \delta_\rho = \frac{\rho_2 - \rho_1}{\rho_2}. \tag{5}$$

Here $R_1$ and $R_2$ are the radii within, and just outside the jump, determined from the estimated radii of wave crests as:

$$R_1 = r_1 - \frac{r_2 - r_1}{2}, \tag{6a}$$

$$R_2 = r_{3,4} + \frac{r_{3,4} - r_{2,3}}{2}, \tag{6b}$$

where the value of $R_2$ depends on the number of waves observed (3 for flow rates 50-150 and 4 for higher ones). In the first set of experiments ($\rho_2 \approx 1.10544$ gcm$^{-3}$) $\delta_\rho \approx 0.097$, and in the second ($\rho_2 \approx 1.05044$ gcm$^{-3}$) $\delta_\rho \approx 0.05$ for all flow rates. According to Eqs. 4 and 6, the flow speed is inversely proportional to the wave radii. When relating this to the distances between the rings (Section 2.2, Fig. 5), it can be seen that as the wave radii increase from the inner to outer wave, the flow slows down.

Since the direct measurements of $H_1$ and $H_2$ were not available, they had to be estimated. The mean thickness of the layer below the interface along which the waves were propagating against the flow, $h$, was calculated in two ways. One was to use the flow rate, $Q$, the time, $t$, and the surface of the tank or pie dish covered with salty water, $(A_1)_{T,P}$. The latter was estimated from the total surface, $(A)_{T,P}$, and $R_1$ as

$$h = \frac{Qt}{(A_1)_{T,P}}, \ (A_1)_{T,P} = (A)_{T,P} - (R_1^2)_{T,P}\pi. \tag{7}$$

The another one, used further in this report, was to numerically estimate $h$ from the dispersion relation for the phase speed ($c$) in two-layer, inviscid fluid (Thorpe, 2005) as

$$c^2 = \frac{g'}{k} tanh[kh], \ \ k = \frac{2\pi}{\lambda}, \tag{8a}$$

where $\lambda$ is the wavelength (estimated as the difference in successive wave radii), and $k$ is the corresponding wave number. This relation is derived taking into consideration the assumptions of small amplitudes of internal waves (i.e. linear displacements), and no velocity shear between the layers (see Eq. 3.4, Thorpe, 2005). Since the observed waves were stationary, the phase speed had to be equal to the flow speed, $U$, given with (4). Then, (8a) becomes:

$$\frac{2\pi Q^2}{g' r^2 \lambda^3} = (kh)^2 \, tanh(kh). \tag{8b}$$

Rewriting Eq. 8 gives $Fr_2 = tanh(kh)/(kh),$ so the values of $Fr_2$ thus obtained are between 0 and 1 (corresponding to the limits for subcritical flow in 2D case). The depth outside the jump, $H_2$, was then taken as $H_2 = h(r = R_2)$. For the depth inside the jump, $H_1$, we took the value of $H_2$ at the first moment when the waves were well-formed, so their radii could have been measured from the photos. This was usually 10 s after the start of experiment in the tank, and 30-35 s in the pie dish (see Section 2.2). Furthermore, it was assumed that $H_1$ remained constant and was never greater than $H_2$.

2. The ratio of outer ($H_2$) and inner ($H_1$) depth of the salty fluid, $q$

$$q = H_2 / H_1 \tag{9}$$

Some of the calculated parameters for $\delta_\rho \approx 0.097$ are plotted in Figures 8-11. The dependence of $R_2$ on $H_2$ (and therefore on $\lambda$) is given in Fig. 8. It can be seen that, independently of the geometry of experiment used (Fig. 8; values in the tank, circles, or in the pie dish, asterisks), we find almost the same values of $R_2$ at the same $H_2$ (i.e. the same wavelengths at the same jump radii) for the given flow rate.

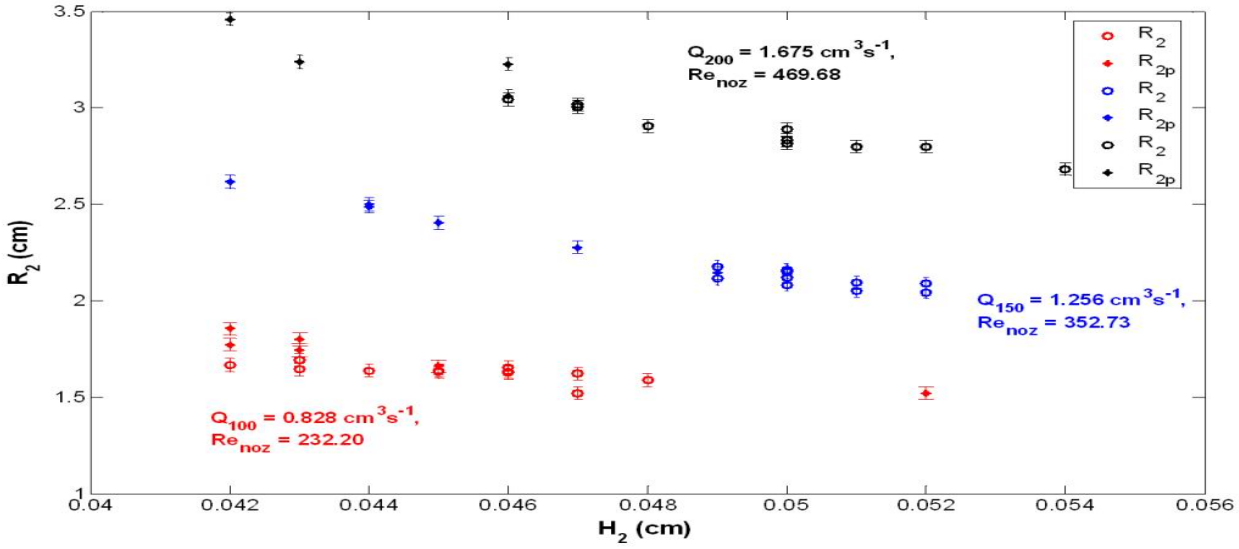


*Figure 8.* Dependence of outer jump radius, $R_2$ (with error bars), on $H_2$ for the pump settings 100 (red), 150 (blue) and 200 (black), for the experiments without (circles) and with the pie dish (asterisks). The rest as in Figure 6.

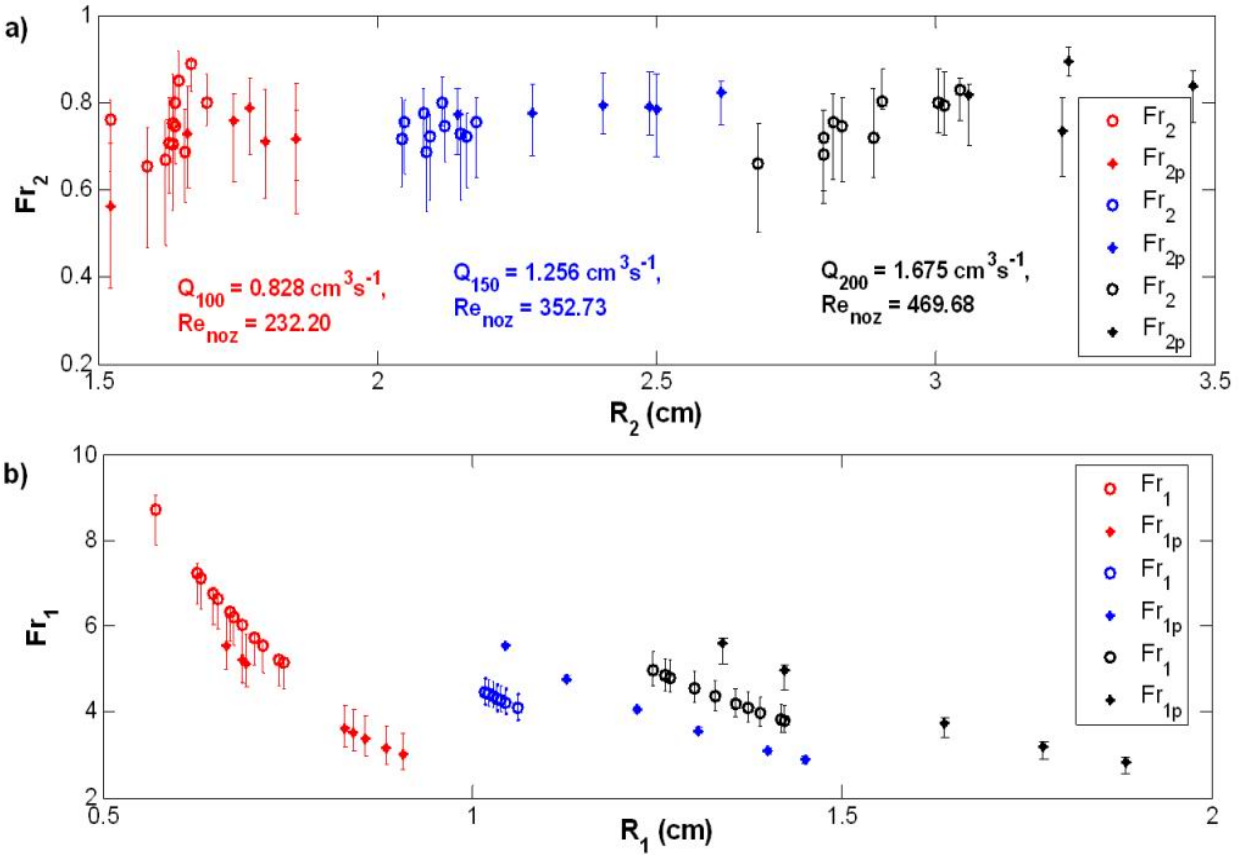


*Figure 9.* a) Downstream Froude number, $Fr_2$ (with error bars), versus outer jump radius, $R_2$; b) upstream Froude number, $Fr_1$ (with error bars), versus inner jump radius, $R_1$. The rest as in Figure 7.

Furthermore, as discussed in Section 2.2, the number of waves does not depend on the experimental geometry. From now on, we will refer to this behaviour of the observed waves as the "dynamical similarity" of wave patterns in the tank and the pie dish. The values of $R_2$ decrease with time (see also Figs. 5 and 6) and $H_2$ increases. The critical values of both $R_2$ and $H_2$, i.e. the values just before the onset of instabilities, seem to grow as the flow rate is increased.

According to Eq. 8, the values of downstream Froude number ($Fr_2$, Fig. 9a) are below 1, and there is no significant correlation with $R_2$. However, the upstream Froude number ($Fr_1$, Fig. 9b) clearly increases as $R_1$ decreases (the jump becoming narrower with time), achieving the maximal values of ≈ 8-10 for the lowest flow rate depicted ($Q_{100}$, red), and ≈ 5-6 for the higher flow rates ($Q_{150}$, blue; $Q_{200}$, black) just before the onset of instabilities (smallest $R_1$).

The time evolution of the depth ratio, $q$, is shown in Fig. 9. This increase of the fluid depth at the jump is more evident in the pie dish (asterisks, dashed lines), reaching values of ≈ 1.1-1.25 before transition to turbulent regime. Also, the values of $q$ are smaller when only the tank is used due to the slower filling. However, these results have to be taken with some caution, since they are calculated from $H_2$, the estimate of which is mostly subject to uncertainties in determining the outer ring radii from photos.

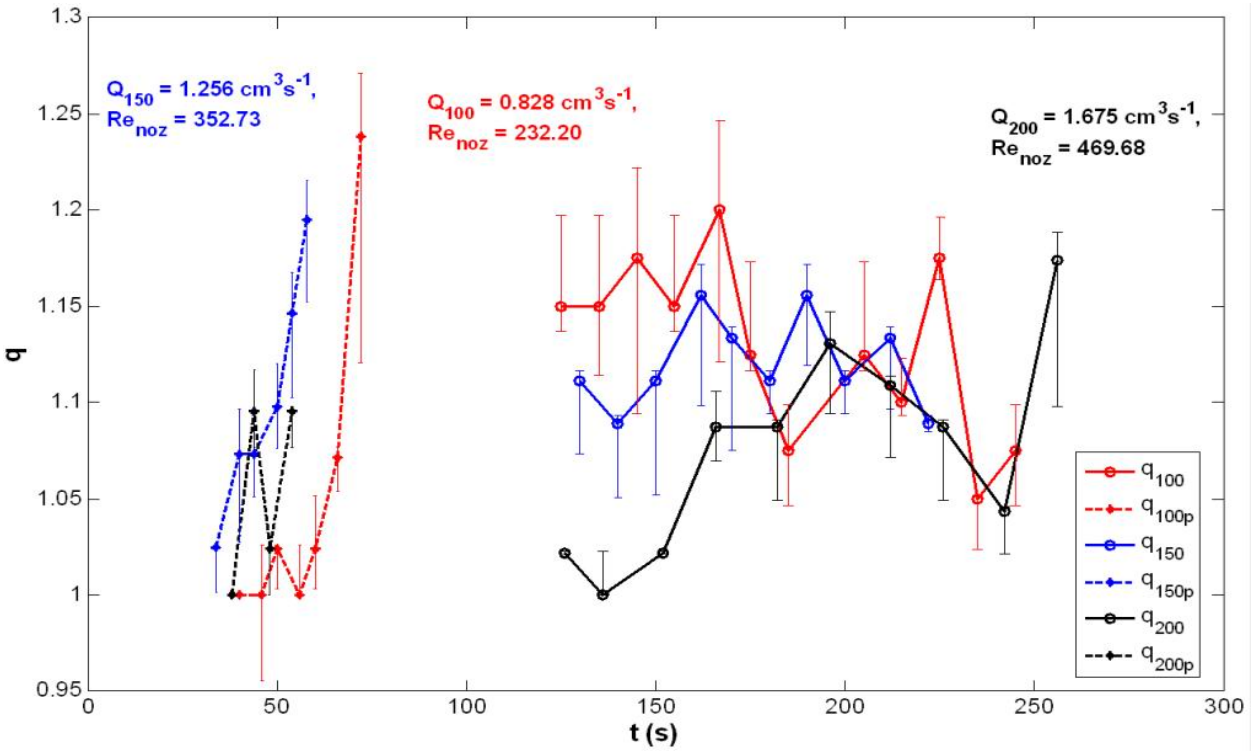


*Figure 10.* Evolution of $q$ (Eq. 9), with error bars, in time. The rest as in Figure 7.

Watson (1964) derived the theoretical prediction of the jump position ($R_1$) in the single-layer, viscous fluid, for both the laminar and turbulent flows. He determined $R_1$ by equating the rate of loss of momentum to the thrust of pressure, not taking into account the surface tension (significant factor in the single-layer fluid but not present here), and assuming that $H_1 << H_2$. He also assumed that the radial width of the jump can be ignored, which may not be the case here (see Fig. 5 for comparison of $r_3$ and $r_1$). His comparison of theory and experiments is repeated here in Fig. 11, i.e. Watson's (1964) Fig. 4, with $a$ being the nozzle radius (here $a_{noz}$), $Re$ the Reynolds number of flow in the nozzle (here $Re_{noz}$), $r_1$ position of the jump (here $R_1$), and $d$ the depth outside the jump (here $H_2$). In two-layer fluid experiments his theoretical relations can be written as (see his Eqs. 41 and 42):

$$A = \frac{R_1}{a_{noz}} Re_{noz}^{-1/3}, \tag{10a}$$

$$B = \frac{R_1 H_2^2 g' a_{noz}^2}{Q^2} + \frac{a_{noz}^2}{2\pi^2 R_1 H_2}. \tag{10b}$$

From Table 1 it can be seen that Reynolds numbers in our experiments are of order of magnitude less than his, due to the lower flow rates used. The observed $R_1$ are here from 0.5 to 2 cm (Fig. 9a), while in his experiments their range is ≈ 2.5-18 cm (1-7 in.). Measurements of $d$ in his experiments gave results of ≈ 0.33-1.65 cm (0.13-0.65 in.), and here $H_2$ was estimated as ≈ 0.04-0.06 cm. The differences between his and our measurements result mainly in shifting our calculated values given in Eq. 9a to the right (Fig. 12) of his theoretical curve (Fig. 11). As for the values of $B$, their range (-1.55 to -2) is close to his values ($\bar{2}.5$ - $\bar{2}$, Fig. 11, equivalent to the span of -1.5 to -2 in Fig. 12), and also with similar, but slower, linear decay. These results indicate that the analogous theoretical relation might also hold for the jump radius of the problem studied here.

Figures 13 and 14 show some of the parameters already calculated using the density $\rho_2 \approx 1.10544$ gcm$^{-3}$ ($\delta_\rho \approx 0.097$) for flow rate $Q_{100}$, but now compared with the results for reduced density of salty water, $\rho_2 \approx 1.05044$ gcm$^{-3}$ ($\delta_\rho \approx 0.05$). We see that the functional dependence of $R_2$ on $H_2$ remains the same, i.e. there is "dynamical similarity" of experiments with and without the pie dish (Fig. 13a, asterisks and circles, respectively). However, the critical values of both $R_2$ and $H_2$ are greater for the lower density of salty water (Fig. 13a, black). There is also clear dependence of upstream Froude number, $Fr_1$, on density difference between salty and fresh water (Fig. 13b). As can be expected from theory (Eqs. 3 and 5), decreasing $\rho_2$ results in increase of critical $Fr_1$ from 8-10 for $\delta_\rho \approx 0.097$ (Fig. 13b, red) to 12-14 for $\delta_\rho \approx 0.05$ (Fig. 13b, black). As before, the values of $Fr_2$ are below 1 and without significant correlation with $R_2$ (not shown).

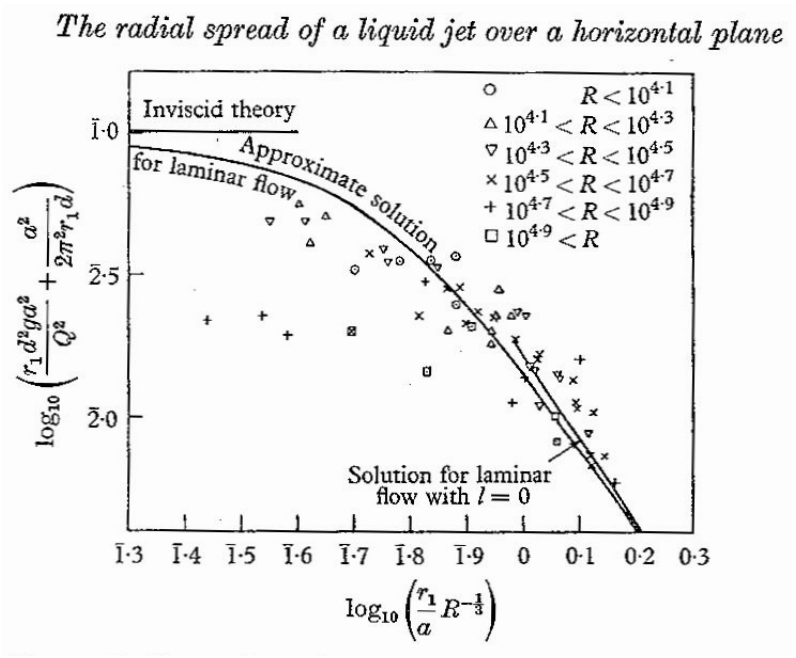


*Figure 11.* Watson's (1964, Fig. 4) comparison of experiment and theory for jump relation (single layer, laminar flow). Here $a$ is the nozzle radius (≈ 0.3 cm), $R$ is the Reynolds number, $g$ is gravity and $d$ is the depth of fluid outside the jump (here corresponding to $H_2$).

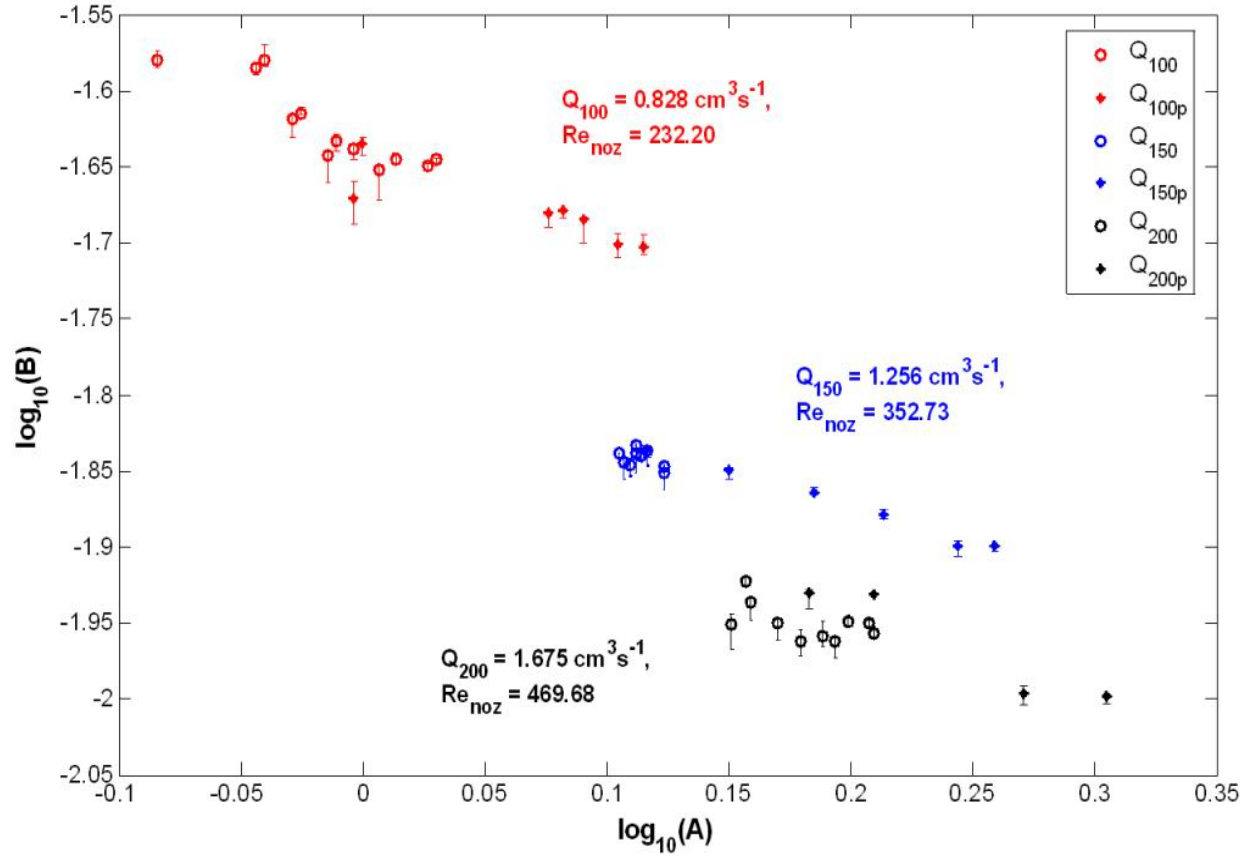


*Figure 12.* Comparison with Watson's results, with error bars (see Fig. 11). The rest as in Figure 6.

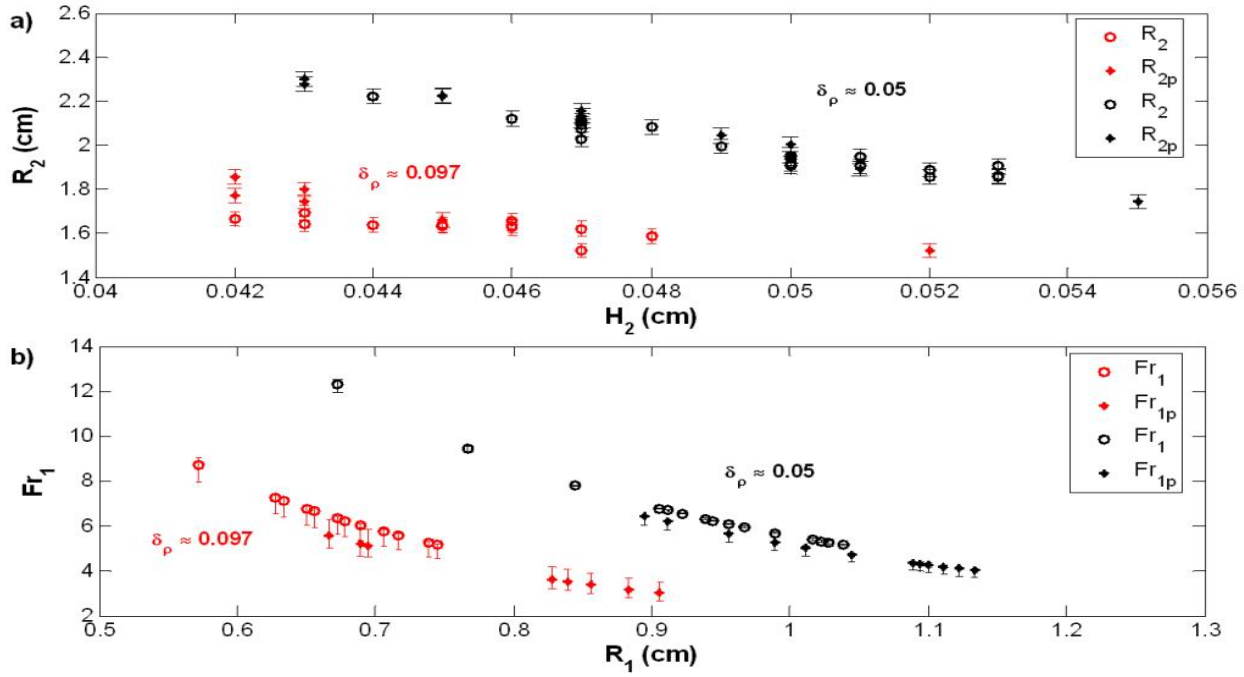


*Figure 13.* a) Dependence of outer jump radius, $R_2$ (with error bars), on $H_2$; b) upstream Froude number, $Fr_1$ (with error bars), versus inner jump radius, $R_1$. Pump setting in both plots is 100 ($Q_{100}$ = 0.828cm$^3$s$^{-1}$, $Re_{noz}$ = 232.20), for the experiments without (circles) and with the pie dish (asterisks). Results for $\rho_2 \approx$ 1.10544 gcm$^{-3}$ ($\delta_\rho \approx 0.097$) are in red, and for $\rho_2 \approx$ 1.05044 gcm$^{-3}$ ($\delta_\rho \approx 0.05$) are in black.

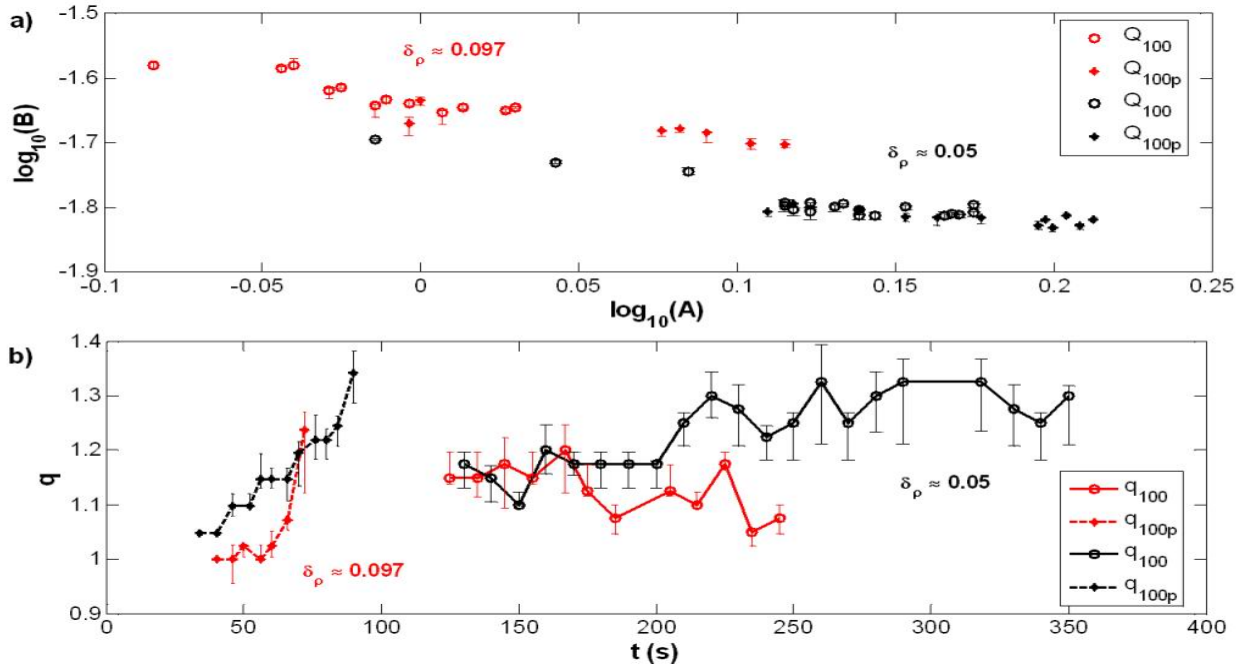


*Figure 14.*a) Comparison with Watson's results, with error bars (see Fig. 11); b) evolution of $q$ (Eq. 9), with error bars, in time. The rest as in Figure 13.

Not only the critical values of $R_2$ (and $R_1$, Fig. 13a) are greater when the density difference is decreased; it is also the case for $q$ (Fig. 14b, black), with values of ≈ 1.3-1.4 for both the pie dish (asterisks, dashed line) and the square tank only (circles, solid line). These increased values affect the theoretical predictions based on Watson's (1964) relations (Eq. 9) by placing the results for $\delta_\rho \approx 0.05$ (Fig. 14a, black) below the ones for $\delta_\rho \approx 0.097$ (Fig. 14a, red).

## 4. Conclusions and recommendations for future experiments

The circular hydraulic jump has been the subject of many theoretical, experimental, and lately numerical studies. Still, many facets of it remain unexplained or unexplored. In this experimental study we tried to describe some of the features of the circular internal jumps in two-layer fluid, and explore the possibility of their occurrence in fluid with continuous stratification.

In the two-layer case, both qualitative behaviour and calculated parameters show dependence on the flow rates and density differences used. Increasing Reynolds number in the nozzle (for the same density difference) or decreasing the density difference between fresh and salty water results in destabilizations of the flow, which can be seen as the cusp-like deformations and narrow, quickly varying, waves within the internal ring of the jump (Fig. 4a and 4b). The onset of instabilities seems to depend more on the density difference than on Reynolds number. Results for upstream Froude numbers (Figs. 9b and 13b) seem to confirm those observations. Although there are differences in values of $R$ and $H$ (and consequently $Fr_1$, Eq. 3) when the pie dish is used in experiments, the overall dynamic behaviour also seems to be similar (Figs. 8 and 13a). The time evolution of jump amplitude $q$ (Eq. 9), although not completely precise because of uncertainties in determining the outer wave radii, still indicates that the maximal values are reached just before the transition into turbulent regime (≈ 1.1-1.4). In all experiments, no clear indication of rotor formation has been observed.

The experiments where the sharp density difference was smoothed by diffusion show no observational evidence of stationary waves (Fig. 7), implying that the stationary, laminar waves cannot occur in continuously stratified fluid. Still, it would be recommendable to further verify these observations by repeating the experiments in fluid with the known (prescribed or measured) density gradient.

The above conclusions for two-layer fluid, however, have to be taken with some caution, because their derivation is based not on measured values of fluid depth, but their estimates from the dispersion relation for inviscid fluid (Eq. 8). The direct measurements of the depth of salty fluid would therefore be

very useful for investigating the role of viscosity, and revealing the jump structure itself. Craik et al. (1981), in their experiments for single-layer fluid, used a laser dye absorption for measurements of the height profile and thus the jump radius. Bloom and Burns (1997) also recommended this method in their experimental report. The method works by scanning a laser perpendicular to the tank bottom, and reading the intensity of transmitted light. The presence of dye in the fluid then makes the amount of light absorbed directly proportional to the fluid height. For the two-layer fluid, the laser should perhaps be aimed through side walls of the tank, and due to differences of refractive indices for salty and fresh water the dye might not be necessary at all.

Ideally, the experiments would have to be conducted in a circular tank, large enough so the circulation caused by the side walls would not significantly affect the jump patterns. Also, the great sensitivity of experiment on disturbances from its surroundings makes it necessary that the support base for the tank is stable, and attenuating vibrations. In this experimental study we have only explored moderate Reynolds numbers (of order $10^2$); it would be worth to explore the behaviour for the higher Reynolds numbers by increasing the radii of nozzles used. Further experimental investigation, as well as the developed theoretical model to verify the observations against, would be very useful in revealing the dynamics of this interesting phenomenon.

**Acknowledgements**

I wish to thank to Steve Thorpe for his guidance and supervision, and especially for his great patience. Keith Bradley is thanked for the help with the experiment. Thanks to the GFD Staff, especially Claudia Cenedese, Jack Whitehead, Jeannie Fleming and Penny Foster for taking such a good care of us.
Thanks to Joe Pedlosky for his interesting lectures, and the esteemed audience (particularly Joe Keller and Ed Spiegel) whose comments made me doubt the things I thought I knew well.
Daphne Thorpe is very much thanked for knowing the importance of good chocolate cakes in times of crisis. George, I doubt I will ever be good in softball, but thank you for trying to teach me.
Finally, to all my fellow Fellows: I hope our paths will cross again some day.

**References**

Bloom C., 1997, *The circular hydraulic jump-pursuit of analytic predictions*, PhD Thesis (University of Texas)

Bloom C. and E. Burns, 1997, *The hydraulic jump-experimental analysis*, Laboratory report (University of Texas)

Bohr, T., P. Dimon and V. Putkaradze, 1993, Shallow-water approach to the circular hydraulic jump, *J. Fluid Mech.* **254**: 635-648.

Bowles, R. I. and F. T. Smith, 1992, The standing hydraulic jump: theory, computations and comparison with experiments, *J. Fluid Mech.* **242**: 145-168.

Bush, J. and J. Aristoff, 2003, The influence of surface tension on the circular hydraulic jump, *J. Fluid Mech.* **489**: 229–238.

Bush, J., J. Aristoff and A. Hosoi, 2006, An experimental investigation of the stability of the circular hydraulic jump, *J. Fluid Mech.* **558**: 33–52.

Craik, A., R. Latham, M. Fawkes and P. Gibbon, 1981, The circular hydraulic jump, *J. Fluid Mech.* **112**: 347–362.

Hassid, S., A. Regev and M. Poreh, 2007, Turbulent energy dissipation in density jumps, *J. Fluid Mech.* **572**: 1–12.

Higuera, F. J., 1994, The hydraulic jump in a viscous laminar flow, *J. Fluid Mech.* **274**: 69-92.

Holland, D. M., R. R. Rosales, D. Stefanica and E. G. Tabak, 2002, Internal hydraulic jumps and mixing in two-layer flows, *J. Fluid Mech.* **470**: 63–83.

Lighthill J., 1978, *Waves in fluids*, Cambridge University Press, 504 pp.

Lord Rayleigh, 1914, On the theory of long waves and bores, *Proc. Roy. Soc. Lond.* **A 90**: 324-328.

Thorpe, S. A., 2005, *The turbulent ocean*, Cambridge University Press, 439 pp.

Thorpe, S. A., 2007, Dissipation in hydraulic transitions in flows through abyssal channels, *J. Mar. Res.* **65 (1)**: 147-168.

Thurnherr, A. M., L. C. St. Laurent, K. G. Speer, J. M. Toole and J. R. Ledwell, 2005, Mixing associated with sills in a canyon on the mid-ocean ridge flank, *J. Phys. Oceanogr.* **35 (8)**: 1370–1381.

Watson, E.J., 1964**,** The radial spread of a liquid jet over a horizontal plane, *J. Fluid Mech.* **20**: 481-499.